International Journal of Greenhouse Gas Control 19 (2013) 471–477

Contents lists available at ScienceDirect

International Journal of Greenhouse Gas Control

journal homepage: www.elsevier.com/locate/ijggc

CO_2 breakthrough and leak-sealing – Experiments on shale and cement

Seunghee Kim [a,*], J. Carlos Santamarina [b,1]

[a] Bureau of Economic Geology, Jackson School of Geosciences, The University of Texas at Austin, University Station, Box X, Austin, TX 78713, USA
[b] School of Civil and Environmental Engineering, Georgia Institute of Technology, 790 Atlantic Drive, N.W., Atlanta, GA 30332, USA

ARTICLE INFO

Article history:
Received 14 March 2013
Received in revised form 3 September 2013
Accepted 6 October 2013
Available online 6 November 2013

Keywords:
CO_2 geological storage
Leakage
Breakthrough pressure
Crack sealing
Fines migration

ABSTRACT

The long-term storage of CO_2 in deep geological formations would lose effectiveness if CO_2 leaks through the cap rock, joints, and improperly grouted wells. Plug tests conducted on shale and cement specimens highlight the importance of hairline cracks in otherwise intact small-pore materials. Crack sealing is attempted under pressure by injecting suspensions of bentonite and kaolin; the sub-micron particles successfully fill cracks, and the CO_2-breakthrough pressure increases significantly above initial values. The sealing strategy can be optimally engineered for field applications during or after CO_2 injection in order to prevent CO_2 leakage.

1. Introduction

Supercritical CO_2 injected in deep formations migrates upwards and accumulates underneath the caprock (Bielinski et al., 2008; Espinoza et al., 2011; Gaus et al., 2008; Okwen et al., 2010). The caprock and cement plugs must exhibit a breakthrough pressure P_{bt} that exceeds the pressure difference between the CO_2 phase P_{CO2} and the water phase P_w, $P_{bt} > P_{CO2}$-P_w (Bergmo et al., 2011; Ehlig-Economides and Economides, 2010; Kopp et al., 2009; Saadatpoor et al., 2009). The pressure difference between the two fluids is a function of the CO_2 pool height P_{CO2}-$P_w = H\cdot(\gamma_w$-$\gamma_{CO2})$, where the pool height H is either controlled by geometric traps or the CO_2 entry pressure in the reservoir rock (Kim and Santamarina, 2013). The breakthrough pressure in seals P_{bt} depends on the shale or cement pore radius r_p [m] and the interfacial tension T_s [mN/m] between water and CO_2, $P_{bt} \approx 2\cdot T_s/r_p$. The characteristic pore radius in shale caprocks is 5 nm < r_p < 100 nm (Armitage et al., 2010; Bachu and Bennion, 2008; Katsube and Williamson, 1994), therefore, the estimated CO_2 breakthrough pressure is between 0.1 MPa and 5 MPa in a fracture-free formation (Hildenbrand et al., 2002, 2004; Li et al., 2005; Wollenweber et al., 2010). Such breakthrough pressures could be expected at most candidate sites for CO_2 geological storage in the absence of discontinuities (Bachu and Bennion, 2008; Doughty et al., 2008; Gaus et al., 2005; Sharma et al., 2009; White et al., 2004). Similarly, the well cement that fills the annulus between the host rock and the casing may resist a CO_2 breakthrough pressure as high as ~1 MPa (Benson and Hepple, 2005; IPCC, 2005).

Discontinuities reflect the formation history. In rocks, discontinuities often relate to bedding planes and the stress history (Hoek and Brown, 1990), have a lower CO_2 breakthrough pressure because of larger interconnected pores in most cases (Downey, 1984), and become preferential conduits for CO_2 leakage (Bildstein et al., 2010; Dooley et al., 2010). Discontinuities along the cement–caprock or cement–casing interfaces could dramatically reduce the seal capacity (Kutchko et al., 2007; Viswanathan et al., 2008; Wigand et al., 2009); in this case, the role of the cement fill is most critical during CO_2 injection when the CO_2 pressure is highest and in the long-term as hydro-chemo-mechanical changes take place.

Several strategies have been proposed to address the risk of CO_2 leakage (Réveillère et al., 2012): (1) control the overpressure of CO_2, (2) enhance CO_2 immobilization in the form of dissolution or capillary trapping, (3) form a hydraulic barrier in the overlaying layer, and (4) modify the fracture hydraulic properties. Attempts to control hydraulic properties of discontinuities have considered microbial clogging (Bryant and Britton, 2008; Cunningham et al., 2009) and the injection of polymer gels (Sydansk et al., 2005). In this research, we investigate the CO_2-breakthrough pressure for caprock shales and cement specimens, and seek to find feasible strategies to effectively plug discontinuities.

* Corresponding author. Tel.: +1 404 805 3724; fax: +1 512 471 0140.
E-mail addresses: simseung@gmail.com, seunghee.kim@beg.utexas.edu (S. Kim), jcs@gatech.edu (J.C. Santamarina).
[1] Tel.: +1 404 894 7605; fax: +1 404 894 2281.

1750-5836/$ – see front matter © 2013 Elsevier Ltd. All rights reserved.
http://dx.doi.org/10.1016/j.ijggc.2013.10.011

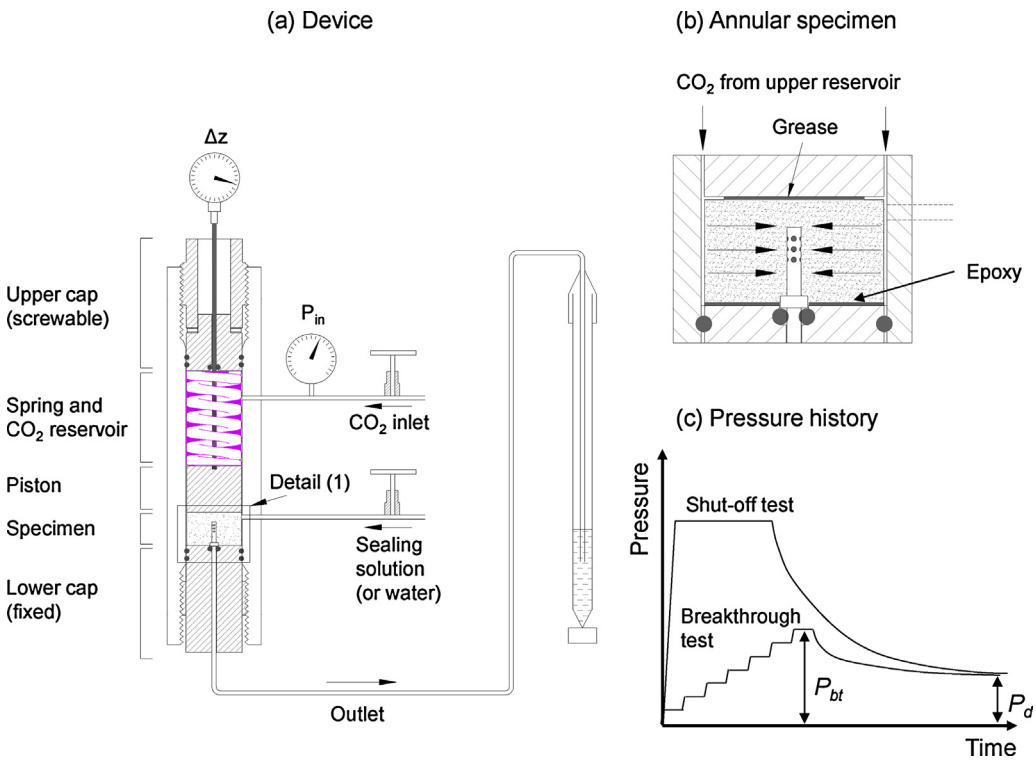

Fig. 1. Experimental device for CO_2-breakthrough and sealing studies. (a) The internal spring applies a constant vertical force onto the specimen. (b) CO_2 infiltrates the specimen radially. (c) Pressure histories typically used for determining breakthrough P_{bt} and shut-off P_d pressures in two different test types.

2. Experimental study

Breakthrough and sealing tests are conducted on core plugs using a uniquely designed device to apply high fluid pressure under constant axial stress.

2.1. Experimental device

The high-pressure cell is shown in Fig. 1a ($P \leq 20$ MPa – details in Espinoza, 2011; Kim, 2012). A high stiffness steel spring housed in the CO_2 reservoir is used to apply a constant force equivalent to a vertical stress up to $\sigma_v \leq 3$ MPa. The test is designed for radial flow to minimize the probability of preferential leak path along the gap between the specimen and the outer sleeve/cell either due to coring damage or poor matching between surfaces in conventional 1-D plug tests (Fig. 1b). The outlet pipe connects to a pipette to measure flow-through water and to detect CO_2 breakthrough. The high-pressure cell has two inlet ports, one for CO_2 and the other to inject either the sealing solution (water-based suspension) or water as needed (Fig. 1a). A pore pressure transducer located next to the CO_2 inlet valve is used to monitor the CO_2 pressure (PX303, OMEGA; output: 0.5–5.5 Vdc, Accuracy: 0.25% FS, maximum pressure reading: 6000 psi). High pressure is reached using gas booster (Haskel AG-75).

2.2. Materials – specimens

Two sets of specimens were tested as part of this study. First, cores of the shale caprock from the southern Kansas CO_2 pilot test site were prepared for the required test geometry (outside diameter $d_c \sim 40$ mm, inside diameter $d_p \sim 3.17$ mm, height 25 mm $< h <$ 35 mm, polished upper and lower faces). Cores belong to Kinderhook–Chattanooga shale group (shale or shaly dolomudstones; porosity $\varphi = 0.04$–0.08; permeability <0.01 md – Watney and Rush, 2013).

The second set of specimens were prepared using class-A well-cement at a water–cement ratio w/c = 0.4. The cement paste was poured into a specifically designed mold to cast specimens of the same dimensions as the shale samples. Cement specimens were cured under 100% humidity, atmospheric pressure and room temperature for 28 days. The specimen porosity measured after curing was $\varphi = 0.4$.

2.3. Sealing strategy

Fines migration and accumulation at pore throats can clog and seal porous media (Khilar and Fogler, 1998; Sharma and Yortsos, 1987; Valdes and Santamarina, 2006, 2008). Herein, we attempt to seal cracks using suspensions of sub micron-size particles in order to decrease the characteristic pore radius r_p within cracks. Suspensions are injected under a constant spring load equivalent to $\sigma_v \sim 1$ MPa, followed by further CO_2 injection (Fig. 1a). The selected water-based suspensions are prepared with bentonite (1gram of GEL-PureGold bentonite, and 20 ml of water; $S_s = 400$–$800\ m^2/g$) and kaolin (1 g SA1-Wilkinson kaolin, 1 g dispersant, and 20 ml of water; $S_s = 10$–$20\ m^2/g$).

2.4. Test procedure

The saturated shale-or-cement specimen was mounted into the high-pressure cell; epoxy was added at the lower interface and grease on the top interface to prevent boundary leaks between the specimen and the stainless steel caps (Fig. 1b). The spring applies a constant force equivalent to a vertical stress equal to $\sigma_v \sim 1$ MPa. Initially, water fills the annulus around the specimen.

Two inlet pressure histories are imposed in this study (note: the outlet pressure is atmospheric in all cases). The first one involves a gradual increase in gas pressure until gas percolates throughout the specimen at the breakthrough pressure P_{bt} (Fig. 1c; Harrington and Horseman, 1999; Horseman et al., 1996; Li et al., 2005; Schowalter,

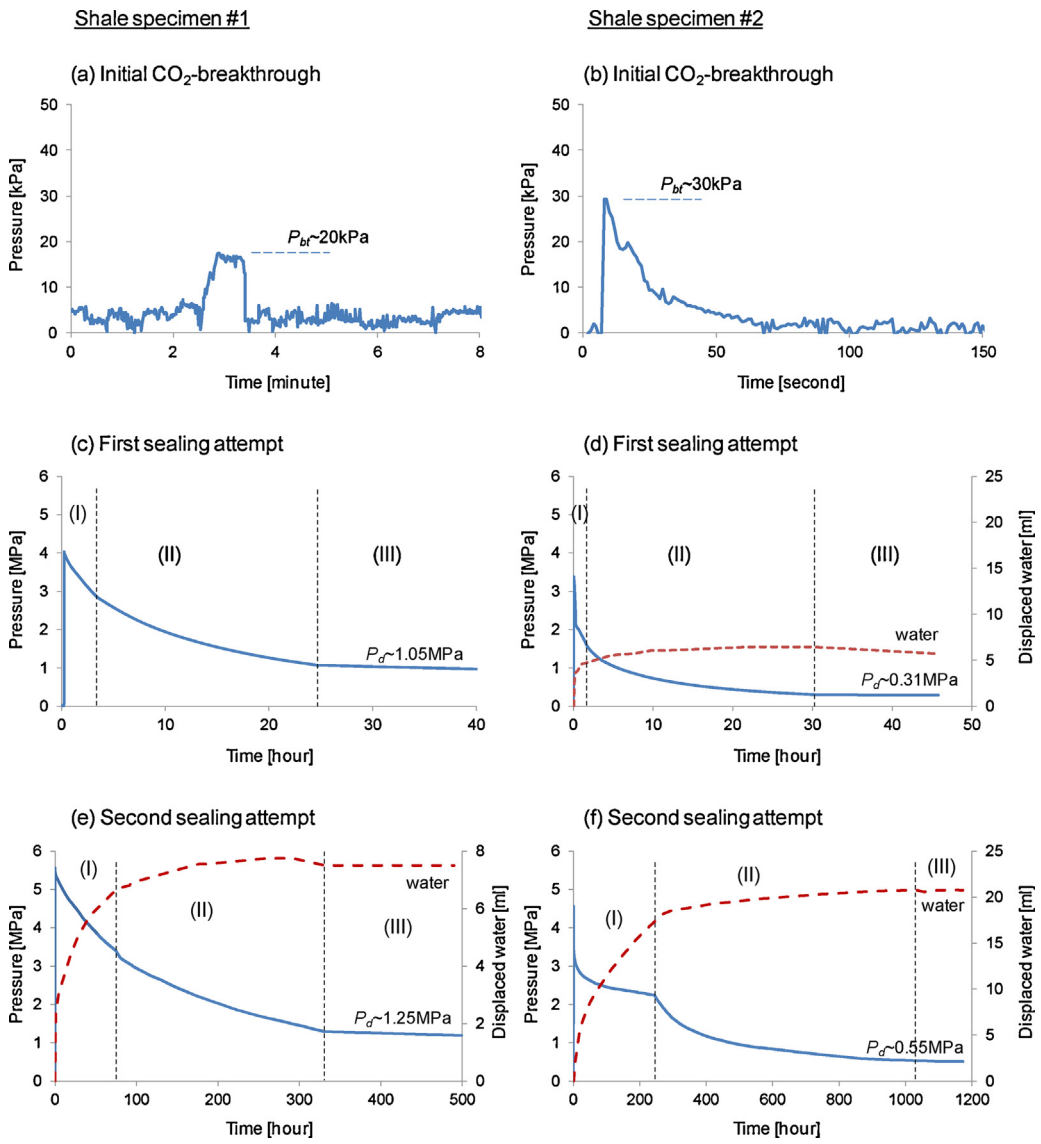

Fig. 2. Shale specimens – test results. (a) and (b) Initial CO_2-breakthrough tests – $P_{bt} \sim 20$ kPa and $P_{bt} \sim 30$ kPa for specimen #1 and #2; (c) and (e). First and second treatments yield $P_d \sim 1.05$ MPa and $P_d \sim 1.25$ MPa for specimen #1; (d) and (f) Treatments yield $P_d \sim 0.31$ MPa and $P_d \sim 0.55$ MPa for specimen #2. Note: the dotted line shows the volume of displaced water. Three different flow regimes are shown: (I) Single-phase water flow regime, (II) CO_2 flow, and (III) Diffusion regime (Amann-Hildenbrand et al., 2012, 2013; Vassenden et al., 2003). The break in the trend marks when the CO_2 first contacts the specimen (transition from I to II) to eventually lead to CO_2 percolation. Thereafter, water flow decreases and preferential CO_2 flow takes place while the CO_2 pressure decreases to the shut-off value (transition from II to III).

1979; Thomas et al., 1968 – Note: this method requires long testing times in intact rocks – Hildenbrand et al., 2002). Breakthrough is confirmed by continuous CO_2 leakage into the outlet pipette.

The second test sequence starts with the injection of ~8 ml of clay slurry under constant equivalent vertical stress $\sigma_v \sim 1$ MPa to flood the specimen (the volume of the annular gap between the test specimen and the high-pressure cell is 4 ml – Fig. 1a and b). Then, we impose a CO_2 pressure significantly higher than the anticipated breakthrough pressure and close the inlet valve. The reservoir pressure decreases as water discharges until the residual shut-off pressure P_d is reached and CO_2 stops flowing. Specimens undergo a series of bentonite or kaolin slurry treatments and CO_2 re-injections.

3. Experimental results

We measure the initial CO_2-breakthrough pressure P_{bt} in the annular plugs, followed by sealing treatments and shut-off pressure measurement. Post-test forensic analyses provide insight into crack sealing and transport mechanisms.

3.1. Shale plugs

3.1.1. Initial CO_2 injection

The three shale specimens exhibited very low CO_2-breakthrough pressures, ranging from $P_{bt} \approx 10$–30 kPa (Fig. 2a and b and Table 1). This pressure range corresponds to 4–6 μm pore radius (from $r_p = 2T_s/P_{bt}$ where the interfacial tension is assumed as $T_s = 60$ mN/m under pressure $P < 1$ MPa), which is much larger than the nano-meter pore radius expected for these shales without cracks. For comparison, CO_2-brine entry pressures between 8 kPa and 464 kPa were estimated for the Chattanooga shale group based on mercury injection data (Watney and Rush, 2013).

3.1.2. Cracks

While visual inspection does not identify cracks (Fig. 3a), careful examination under the microscope reveals the presence of hairline

Table 1
Summary of the CO_2 breakthrough tests and sealing treatments – Shale and cement specimens.

Specimen	Breakthrough pressure	Shut-off pressure		Remarks
	Initial (P_{bt} [MPa])	1st sealing (P_d [MPa])	Final sealing (P_d [MPa])	
Shale #1	0.019	1.05	1.25	Bentonite (1st–2nd) slurry
Shale #2	0.030	0.31	0.55	Bentonite (1st–2nd) & kaolin (3rd)
Shale #3	0.010	0.50	0.58	Bentonite (1st–2nd) & kaolin (3rd)
Cement #1	–	6.15		No sealing treatment
Cement #2	–	0.93		No sealing treatment
Cement #3	–	1.85		No sealing treatment

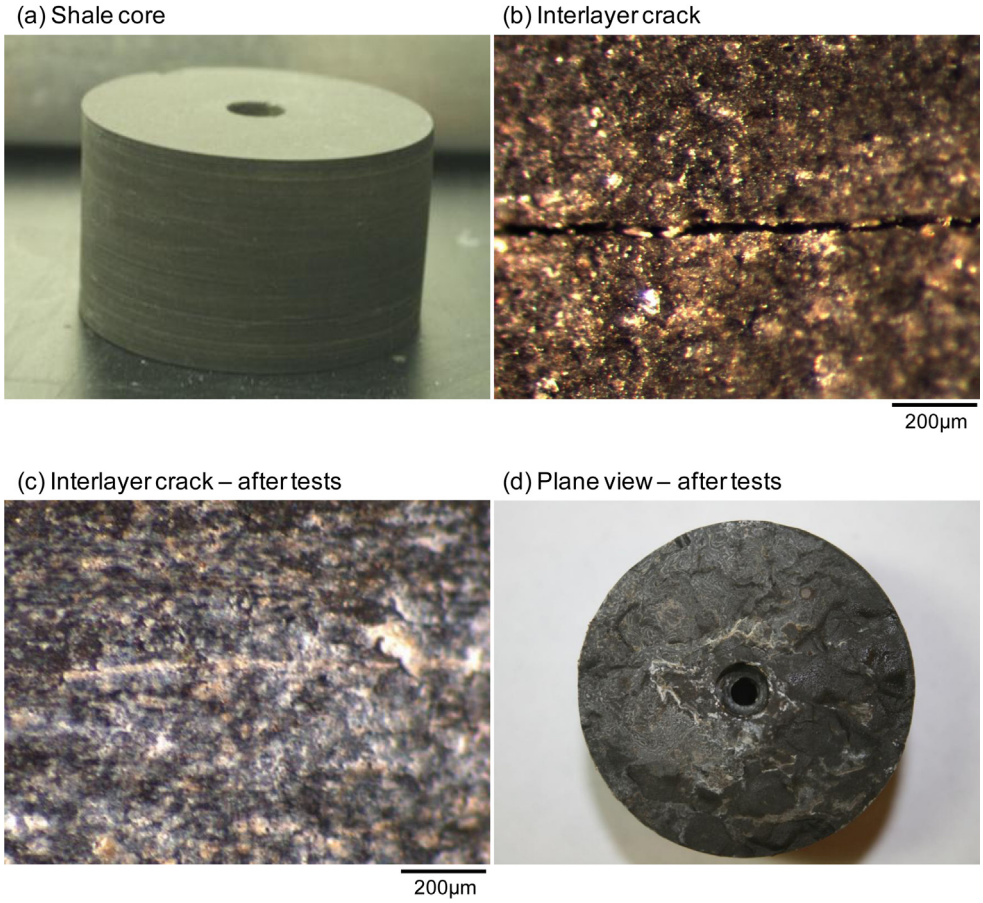

Fig. 3. Shale specimens. (a) Core prepared for the CO_2-breakthrough test. (b) Microscopic image of interlayer crack. Post-test forensic analyses: (c) the microphotograph shows a crack filled with sub-micron bentonite particles after sealing treatments; (d) sub-micron particles deposited in the gap between cracks after sealing treatments.

cracks parallel to the bedding planes in all shale plugs (Fig. 3b). These cracks may have developed during coring and stress relaxation, and are parallel to the imposed flow direction in our test.

3.1.3. Sealing treatment

Specimens underwent a series of bentonite or kaolin slurry treatments and CO_2 re-injections during sealing treatments. Trends in Fig. 2 and key values summarized in Table 1 show a marked increase in break-through pressure, and much lower water production and pressure decline rates after successive treatments. The water produced is transparent, without clays in suspension.

There is a concurrent change in pressure–time and flow–time trends (Fig. 2c–f). This point marks the transition from (I) a single-phase water/suspension flow regime to (II) a mixed fluid condition when CO_2 contacts the specimen eventually leading to continuous gas flow at the breakthrough pressure P_{bt} (Amann-Hildenbrand et al., 2012, 2013; Boulin et al., 2011; Vassenden et al., 2003). Being a water-wet rock, water re-imbibition works against the percolating gas until it shuts off the last connected pore-throat. The residual shut-off pressure P_d is lower than the breakthrough pressure (see also Amann-Hildenbrand et al., 2012; Vassenden et al., 2003).

3.1.4. Forensic analyses

The microphotograph in Fig. 3 shows hairline cracks filled with the sub-micron clay particles (compare Fig. 3b with c). Fractures were forced open in tensions to observe the conditions on fracture surfaces. Surfaces show clay deposition in the form of clogging rings (Fig. 3d; see Valdes and Santamarina, 2006, 2007).

3.2. Cement plugs

Three cement specimens were tested to assess their sealing capacity (Table 1). There are no visible cracks in these specimens.

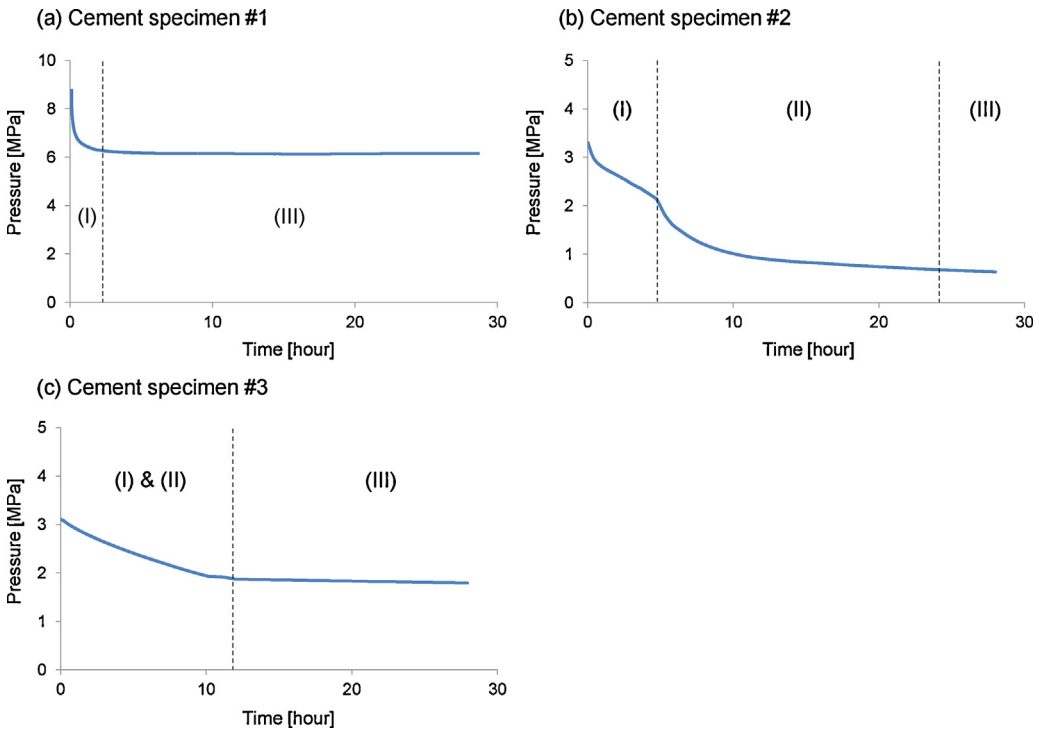

Fig. 4. Cement specimens – Shut-off pressures observed with three different specimens. Note: only specimen #2 exhibits a clear transition from single-phase water flow to CO_2 flow.

3.2.1. Breakthrough and shut-off pressures

The "cement #1" plug showed no CO_2 breakthrough up to 20 MPa. The decline in reservoir pressure results from gas dissolution and diffusive transport (Fig. 4a). For reference, the end pressure $P \sim 6.15$ MPa corresponds to a characteristic pore radius $r_p \sim 11$ nm (assuming $T_s \approx 35$ mN/m at $P \sim 6.15$ MPa).

CO_2 percolated the other two specimens at $P_{bt} \sim 4$ MPa. The "cement #2" plug exhibits a transition from (I) single-phase water flow to (II) gas flow near $P \sim 2$ MPa (Fig. 4b). The change in flow regime is less clear for the "cement #3" plug (Fig. 4c). The shut-off pressures for these two specimens were $P_d \sim 0.93$ MPa and $P_d \sim 1.85$ MPa (Table 1); these values correspond to characteristic pore radii $r_p \sim 75$ nm and $r_p \sim 38$ nm. For reference, the reported mean pore radius for hardened cement pastes ranges between $r_{mean} = 10$ nm and 50 nm (Kondraivendhan and Bhattacharjee, 2010; Reinhardt and Gaber, 1990; Rimmelé et al., 2008).

3.2.2. Forensic analyses

Microscopy and XRD analyses show that decoloration zones on the specimen periphery correspond to cement carbonation (orange color in Fig. 5a & XRD analysis in Fig. 5c). In the absence of advection, diffusive transport limits the carbonation front to a shallow skin thickness in short-duration tests (1–7 mm thick skin – Brandvoll et al., 2009; Kutchko et al., 2007; Rimmelé et al., 2008). The diffusion of CO_2 along mineral boundaries created reaction rims around grains (Fig. 5b); previous studies suggest that these reaction rims result from reactions between calcium silicate hydrate C–S–H and calcium hydroxide $Ca(OH)_2$ with hydrogen ions H^+ and bicarbonate HCO_3^- (Duguid et al., 2011; Liteanu and Spiers, 2011; Wigand et al., 2009). The cement–casing and cement–rock interfaces can develop preferential leakage paths during curing or later during operation due to various hydro-chemo-thermo-mechanically coupled effects emerge.

4. Discussion

Shut-off takes place as water re-imbibition closes pores, starting with the smallest pores first (Hildenbrand et al., 2002; Note: CO_2 is water-saturated in these tests and does not dry the formation). Therefore, both breakthrough and shut-off pressures reflect the smallest pore along the percolating path. As observed in this study, the shut-off pressure P_d is lower than the breakthrough pressure P_{bt} in most cases due to hindered water re-imbibition (Hildenbrand et al., 2002). Therefore, the shut-off pressure is a conservative estimate for the sealing capacity of the caprock.

Well cements may experience 3–5% volumetric shrinkage during curing (Sabins and Rozieres, 1995). A cement annulus thickness t_a that experiences a radial shrinkage strain ε_r could develop a gap $t_{gap} = t_a \cdot \varepsilon_r$ at the cement–casing or cement–rock interface; for example, for $t_a = 10$ mm and $\varepsilon_r = 0.01$, the gap could be as wide as 100 μm. This gap is much larger than the characteristic pore radius of cements tested in this study, the breakthrough pressure would be as low as $P_{gap} = T_s/t_{gap} \approx 1$ kPa, and the gap would become a preferential leakage path. This may explain the high incidence of gas leakage from production wells reported in Alberta, Canada and the North Sea (4.6% for Alberta and 13–19% for North Sea – Nygaard, 2010). Other gap-formation processes include thermal contractions, fluid-driven elastic deformations, and chemical reactions.

Injected aqueous or CO_2-based suspensions must satisfy stability requirements (e.g., use of dispersant or even buoyant particles) and geometric considerations. By extension of standard filter criteria, permeation through the reservoir requires the largest grains in suspension, say the 85% percentile by mass $d^{sus}{}_{85}$, to be significantly smaller than the smaller pores in the reservoir, e.g. the 15% percentile by volume $D^{res}{}_{15}$. Conversely, the aperture of the discontinuity A_{crack} cannot be much larger than the largest grains in the suspension or bridging and clogging will not take place (in the absence of electrochemical effects). We can hypothesize that

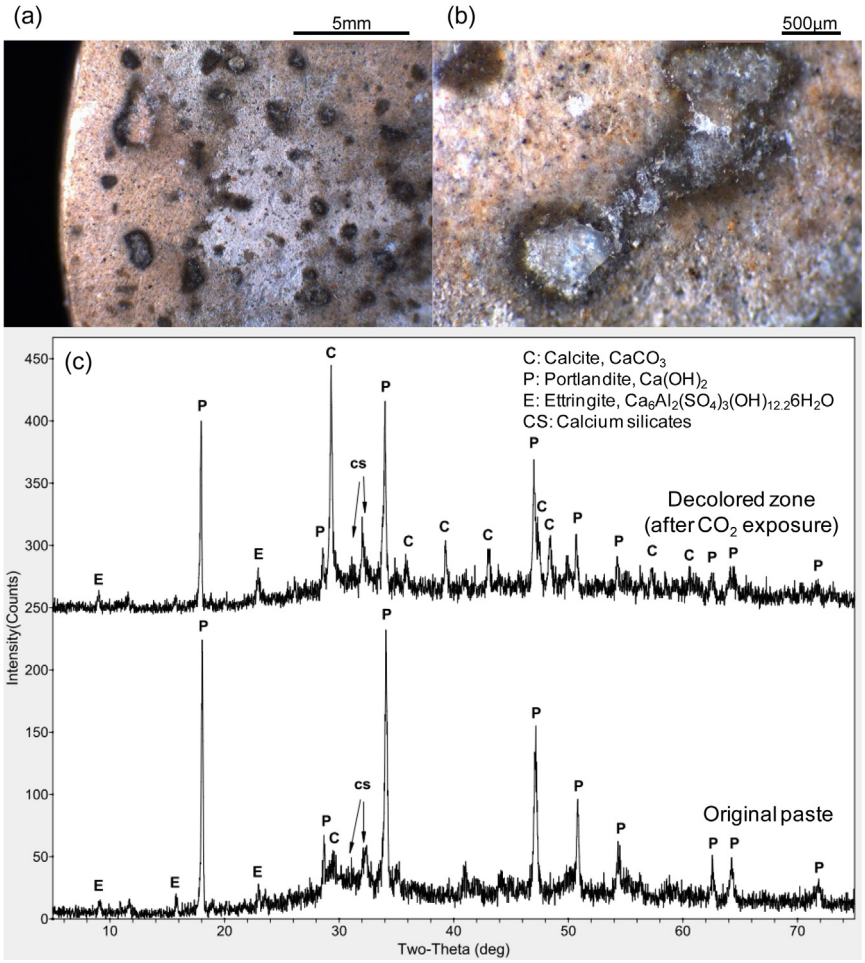

Fig. 5. Cement specimens – Post-test forensic analyses. (a) Carbonation on the specimen peripheral surface (orange color). (b) Reaction rim around grains. (c) XRD analysis for the original cement paste and after exposure to CO_2. (For interpretation of the references to color in this figure legend, the reader is referred to the web version of this article.)

(Kenney et al., 1985; Terzaghi, 1936; Tomlinson and Vaid, 2000; Valdes and Santamarina, 2008):

$$A_{crack} \leq 5 \cdot d_{85}^{sus} \text{ for crack plugging} \quad (1)$$

$$d_{85}^{sus} \leq \frac{D_{15}^{sus}}{10} \text{ for permeation through the reservoir} \quad (2)$$

5. Conclusions

Caprocks and well-cement seal reservoirs to contain injected CO_2; similar applications include gas storage and compressed air. While pores in shales and cements are in the nm-scale and can sustain MPa-scale capillary pressures, orders of magnitude lower breakthrough pressures are measured when specimens contain micron-thick discontinuities.

Suspensions of sub-micron clay particles can be injected to fill cracks. Sealing treatments cause a marked increase in the shut-off pressure, and a pronounced decrease in leak rates can be attained as the specimen is subjected to successive sealing treatments. In particular, shales with hairline cracks can experience an increase in breakthrough pressure from ~30 kPa before treatment to more than $P \sim 1$ MPa after sealing treatments with clay slurries.

Intact cement plugs can sustain a shut-off pressure in excess of $P_d \sim 6$ MPa. Extensive carbonation and reaction rims around grains are readily observed in short-duration tests where water saturated cement plugs are exposed to supercritical CO_2. Reactions should be slower once CO_2 dries the cement.

The design of suspensions for field applications must take crack aperture and reservoir permeation into consideration. The use of dispersants or buoyant particles would extend the reach of suspension-based sealing.

Acknowledgments

Support for this research was provided by the U.S. Department of Energy project DE-FE0001826. We are grateful to insightful comments by anonymous reviewers. Any opinion, findings, conclusions, or recommendations expressed herein are those of the authors and do not necessarily reflect the views of funding organizations. F. J. Santamarina edited earlier versions of the manuscript.

References

Amann-Hildenbrand, A., Bertier, P., Busch, A., Krooss, B.M., 2013. Experimental investigation of the sealing capacity of generic clay-rich caprocks. International Journal of Greenhouse Gas Control In print.

Amann-Hildenbrand, A., Ghanizadeh, A., Krooss, B.M., 2012. Transport properties of unconventional gas systems. Marine and Petroleum Geology 31, 90–99.

Armitage, P.J., Worden, R.H., Faulkner, D.R., Aplin, A.C., Butcher, A.R., Iliffe, J., 2010. Diagenetic and sedimentary controls on porosity in Lower Carboniferous fine-grained lithologies, Krechba field Algeria: a petrological study of a caprock to a carbon capture site. Marine and Petroleum Geology 27, 1395–1410.

Bachu, S., Bennion, B., 2008. Effects of in-situ conditions on relative permeability characteristics of CO_2-brine systems. Environmental Geology 54, 1707–1722.

Benson, S.M., Hepple, R.P., 2005. Detection and options for remediation of leakage from underground CO_2 storage projects. In: Wilson, M., Morris, T., Gale,

J., Thambimuthu, K. (Eds.), Proceeding of the 7th International Conference on Greenhouse Gas Technologies (GHGT7), II. Elsevier, Vancouver, pp. 1329–1335.
Bergmo, P.E.S., Grimstad, A.-A., Lindeberg, E., 2011. Simultaneous CO_2 injection and water production to optimise aquifer storage capacity. International Journal of Greenhouse Gas Control 5, 555–564.
Bielinski, A., Kopp, A., Schutt, H., Class, H., 2008. Monitoring of CO_2 plumes during storage in geological formations using temperature signals: Numerical investigation. International Journal of Greenhouse Gas Control 2, 319–328.
Bildstein, O., Kervévan, C., Lagneau, V., Delaplace, P., Crédoz, A., Audigane, P., Perfetti, E., Jacquemet, N., Jullien, M., 2010. Integrative modeling of caprock integrity in the context of CO_2 storage: evolution of transport and geochemical properties and impact on performance and safety assessment. Oil & Gas Science and Technology – Revue de l'Institut Français du Pétrole 65, 485–502.
Boulin, P.F., Bretonnier, P., Vassil, V., Samouillet, A., Fleury, M., Lombard, J.M., 2011. Entry pressure measurements using three unconventional experimental methods. In: International Symposium of the Society of Core Analysts, Austin, Texas, USA, pp. 18–21.
Brandvoll, Ø., Regnault, O., Munz, I.A., Iden, I.K., Johansen, H., 2009. Fluid–solid interactions related to subsurface storage of CO_2 experimental tests of well cement. Energy Procedia 1, 3367–3374.
Bryant, S., Britton, L., 2008. Mechanistic Understanding of Microbial Plugging for Improved Sweep Efficiency. US DOE NETL, Report DE-FC26-04NT15524.
Cunningham, A.B., Gerlach, R., Spangler, L., Mitchell, A.C., 2009. Microbially enhanced geologic containment of sequestered supercritical CO_2. Energy Procedia 1, 3245–3252.
Dooley, J.J., Trabucchi, C., Patton, L., 2010. Design considerations for financing a national trust to advance the deployment of geologic CO_2 storage and motivate best practices. International Journal of Greenhouse Gas Control 4, 381–387.
Doughty, C., Freifeld, B.M., Trautz, R.C., 2008. Site characterization for CO_2 geologic storage and vice versa: the Frio brine pilot, Texas, USA as a case study. Environmental Geology 54, 1635–1656.
Downey, M.W., 1984. Evaluating seals for hydrocarbon accumulations. AAPG Bulletin 68, 1752–1763.
Duguid, A., Radonjic, M., Scherer, G.W., 2011. Degradation of cement at the reservoir/cement interface from exposure to carbonated brine. International Journal of Greenhouse Gas Control 5, 1413–1428.
Ehlig-Economides, C., Economides, M.J., 2010. Sequestering carbon dioxide in a closed underground volume. Journal of Petroleum Science and Engineering 70, 123–130.
Espinoza, D.N., 2011. Carbon Geological Storage – Underlying Phenomena and Implications. Civil and Environmental Engineering, Georgia Institute of Technology, Atlanta.
Espinoza, D.N., Kim, S., Santamarina, J.C., 2011. CO2 geological storage—geotechnical implications. KSCE Journal of Civil Engineering 15, 707–719.
Gaus, I., Audigane, P., Andre, L., Lions, J., Jacquemet, N., Durst, P., Czernichowski-Lauriol, I., Azaroual, M., 2008. Geochemical and solute transport modelling for CO_2 storage, what to expect from it? International Journal of Greenhouse Gas Control 2, 605–625.
Gaus, I., Azaroual, M., Czernichowski-Lauriol, I., 2005. Reactive transport modelling of the impact of CO_2 injection on the clayey cap rock at Sleipner (North Sea). Chemical Geology 217, 319–337.
Harrington, J.F., Horseman, S.T., 1999. Gas transport properties of clays and mudrocks. Geological Society, London 158, 107–124 (Special Publications).
Hildenbrand, A., Schlömer, S., Krooss, B., Littke, R., 2004. Gas breakthrough experiments on pelitic rocks: comparative study with N_2, CO_2 and CH_4. Geofluids 4, 61–80.
Hildenbrand, A., Schlömer, S., Krooss, B.M., 2002. Gas breakthrough experiments on fine-grained sedimentary rocks. Geofluids 2, 3–23.
Hoek, E., Brown, E.T., 1990. Underground Excavations in Rock. Spon Press.
Horseman, S.T., Harrington, J.F., Sellin, P.,1996. Gas migration in Mx80 buffer bentonite. In: MRS Proceedings. Cambridge University Press.
IPCC, 2005. IPCC special report on carbon dioxide capture and storage. In: Metz, B., Davidson, O., de Coninck, H.C., Loos, M., Meyer, L.A. (Eds.), Prepared by Working Group III of the Intergovernmental Panal on Climate Change. Cambridge University Press, Cambridge, UK and New York, USA, p. 442.
Katsube, T.J., Williamson, M.A., 1994. Effects of diagenesis on shale nano-pore structure and implications for sealing capacity. Clay Minerals 29, 451–461.
Kenney, T.C., Chahal, R., Chiu, E., Ofoegbu, G.I., Omange, G.N., Ume, C.A., 1985. Controlling constriction sizes of granular filters. Canadian Geotechnical Journal 22, 32–43.
Khilar, K.C., Fogler, H.S., 1998. Migrations of fines in porous media. Springer.
Kim, S., 2012. CO_2 Geological Storage: Hydro-Chemo-Mechanically Coupled Phenomena and Engineered Injection. Civil and Environmental Engineering, Georgia Institute of Technology, Atlanta, pp. 188.
Kim, S., Santamarina, J.C., 2013. CO_2 geological storage: hydro-chemo-mechanical analyses and implications. (Under review).
Kondraivendhan, B., Bhattacharjee, B., 2010. Effect of age and water-cement ratio on size and dispersion of pores in ordinary portland cement paste. ACI Materials Journal, 107.
Kopp, A., Class, H., Helmig, R., 2009. Investigations on CO_2 storage capacity in saline aquifers: part 1. Dimensional analysis of flow processes and reservoir characteristics. International Journal of Greenhouse Gas Control 3, 263–276.
Kutchko, B.G., Strazisar, B.R., Dzombak, D.A., Lowry, G.V., Thaulow, N., 2007. Degradation of well cement by CO_2 under geologic sequestration conditions. Environmental Science & Technology 41, 4787–4792.
Li, S., Dong, M., Li, Z., Huang, S., Qing, H., Nickel, E., 2005. Gas breakthrough pressure for hydrocarbon reservoir seal rocks: implications for the security of long-term CO_2 storage in the Weyburn field. Geofluids 5, 326–334.
Liteanu, E., Spiers, C.J., 2011. Fracture healing and transport properties of wellbore cement in the presence of supercritical CO_2. Chemical Geology 281, 195–210.
Nygaard, R., 2010. Well Design and Well Integrity. University of Calgary.
Okwen, R.T., Stewart, M.T., Cunningham, J.A., 2010. Analytical solution for estimating storage efficiency of geologic sequestration of CO_2. International Journal of Greenhouse Gas Control 4, 102–107.
Reinhardt, H.W., Gaber, K., 1990. From pore size distribution to an equivalent pore size of cement mortar. Materials and Structures 23, 3–15.
Réveillère, A., Rohmer, J., Manceau, J.C., 2012. Hydraulic barrier design and applicability for managing the risk of CO_2 leakage from deep saline aquifers. International Journal of Greenhouse Gas Control 9, 62–71.
Rimmelé, G., Barlet-Gouédard, V., Porcherie, O., Goffé, B., Brunet, F., 2008. Heterogeneous porosity distribution in Portland cement exposed to CO_2-rich fluids. Cement and Concrete Research 38, 1038–1048.
Saadatpoor, E., Bryant, S.L., Sepehrnoori, K., 2009. Effect of capillary heterogeneity on buoyant plumes: a new local trapping mechanism. Energy Procedia 1, 3299–3306.
Sabins, F., Rozieres, D., 1995. Shrinkage and Expansion in Oil Well Cements. API Work Group on Shrinkage.
Schowalter, T.T., 1979. Mechanics of secondary hydrocarbon migration and entrapment. Aapg Bulletin-American Association of Petroleum Geologists 63, 723–760.
Sharma, M., Yortsos, Y., 1987. Fines migration in porous media. AIChE Journal 33, 1654–1662.
Sharma, S., Cook, P., Berly, T., Lees, M., 2009. The CO_2CRC Otway project: overcoming challenges from planning to execution of Australia's first CCS project. Energy Procedia 1, 1965–1972.
Sydansk, R.D., Xiong, Y., Al-Dhafeeri, A.M., Schrader, R.J., Seright, R.S., 2005. Characterization of partially formed polymer gels for application to fractured production wells for water-shutoff purposes. SPE Production & Facilities 20, 240–249.
Terzaghi, K., 1936. Arching in sands. Engineering News-Record 116, 690–693.
Thomas, L.K., Katz, D.L., Tek, M.R., 1968. Threshold pressure phenomena in porous media. Old SPE Journal 8, 174–184.
Tomlinson, S.S., Vaid, Y.P., 2000. Seepage forces and confining pressure effects on piping erosion. Canadian Geotechnical Journal 37, 1–13.
Valdes, J.R., Santamarina, J.C., 2006. Particle clogging in radial flow: microscale mechanisms. SPE Journal 11, 193–198.
Valdes, J.R., Santamarina, J.C., 2007. Particle transport in a nonuniform flow field: retardation and clogging. Applied Physics Letters 90, 244101–1244101.
Valdes, J.R., Santamarina, J.C., 2008. Clogging: bridge formation and vibration-based destabilization. Canadian Geotechnical Journal 45, 177–184.
Vassenden, F., Sylta, Ø., Zwach, C., 2003. Secondary migration in a 2D visual laboratory model. In: European Association of Geoscientists & Engineers (EAGE) Conference "Fault and Top Seals: What Do We Know and Where Do We Go?", Montpellier France.
Viswanathan, H.S., Pawar, R.J., Stauffer, P.H., Kaszuba, J.P., Carey, J.W., Olsen, S.C., Keating, G.N., Kavetski, D., Guthrie, G.D., 2008. Development of a hybrid process and system model for the assessment of wellbore leakage at a geologic CO_2 sequestration site. Environmental Science & Technology 42, 7280–7286.
Watney, W.L., Rush, J., 2013. Modeling CO_2 sequestration in saline aquifer and depleted oil reservoir to evaluate regional CO_2 sequestration potential of Ozark Plateau Aquifer System. In: South-Central Kansas, 13th Quarterly Progress Report.
White, D.J., Burrowes, G., Davis, T., Hajnal, Z., Hirsche, K., Hutcheon, I., Majer, E., Rostron, B., Whittaker, S., 2004. Greenhouse gas sequestration in abandoned oil reservoirs: the International Energy Agency Weyburn pilot project. GSA today 14, 4–10.
Wigand, M., Kaszuba, J.P., Carey, J.W., Hollis, W.K., 2009. Geochemical effects of CO2 sequestration on fractured wellbore cement at the cement/caprock interface. Chemical Geology 265, 122–133.
Wollenweber, J., Alles, S., Busch, A., Krooss, B.M., Stanjek, H., Littke, R., 2010. Experimental investigation of the CO_2 sealing efficiency of caprocks. International Journal of Greenhouse Gas Control 4, 231–241.